A New Method for Diagramming Fatigue Strength of Metals Based on the Equivalent Stress Ratio Parameter and Characterization of Fatigue Strength Diagrams

Hiroshi Matsuno

Department of Mechanical Engineering, Sojo University
Ikeda 4-22-1, Kumamoto 860-0082, Japan

email;hi-matsuno@par.odn.ne.jp

Keywords: Hypothesis of plastic adaptation, Equivalent stress ratio, Nominal stress ratio, Stress concentration factor, Fatigue strength diagram, Fatigue strength σ_{w1}, Fatigue strength σ_{w1}

Abstract. In the present paper, equivalent stress ratios (R_{EQ}-ratios) which have been proposed as parameters for correspondence between cyclic stress conditions of notched and unnotched specimens are reviewed, and a method for diagramming fatigue strength of metals based on the parameter of R_{EQ}-ratios is newly proposed. The relation between R_{EQ}-ratios and notch-root-concentrated stress ranges at fatigue strength can be represented by a consistent curve in spite of difference of specimen types (plates and round-bars), loading types (axial, bending, torsion and their combined loads) and stress concentration factors of notches. Accordingly, it can be thought that the relation diagrammed with the R_{EQ}-ratio vs. notch-root-concentrated stress ranges at the fatigue strength represents the intrinsic characteristics of material itself. Fatigue strength diagrams are characterized by two characters of σ_{w1} and σ_{w2}. A proposed method for diagramming is applied to fatigue problems of heat- and surface-treated materials.

Introduction

An author has proposed equivalent stress ratios (R_{EQ}-ratios) as parameters for correspondence between cyclic stress conditions of notched and unnotched specimens. Diagramming relations between R_{EQ}-ratios and notch-root-concentrated stress ranges at fatigue strength, consistent diagrams proper to material can be represented in spite of differences of specimen types (plates and round- bars), loading types (axial, bending, torsion and their combined loads) and notch stress concentration factors. In other words, the relations diagrammed with the R_{EQ}-ratios vs. notch-root-concentrated stress ranges at fatigue strength represent the characteristics on fatigue strength of unnotched specimens themselves. In the present study, a fundamental concept and formulation on parameter of R_{EQ}-ratios is reviewed and a method for diagramming fatigue strength based on the parameter is newly proposed. Experimental data on fatigue strength of the notched and unnotched specimens are widely picked up from literature and plotted on the diagrams of R_{EQ}-ratios vs. notch-root-concen- trated stress ranges ($\Delta\sigma_{NR}$). Fatigue strength diagrams are characterized by two characters of σ_{w1} and σ_{w2}. A proposed method for diagramming is applied to fatigue problems of heat- and surface-treated materials.

A Fundamental Concept and Equations for Fatigue Strength Diagramming

A hypothesis of plastic adaptation and modelling. An author has proposed a hypothesis of plastic adaptation in order to interpret plastic deformation behaviour inherent in fatigue of metals from a

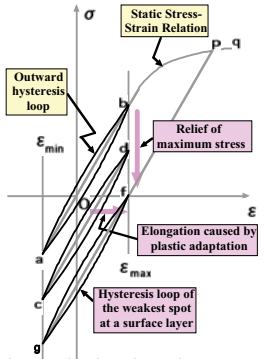

Fig. 1 Plastic adaptation at a surface layer.

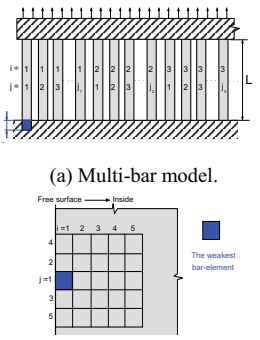

(a) Multi-bar model.

(b) Disposition of bar-elements.

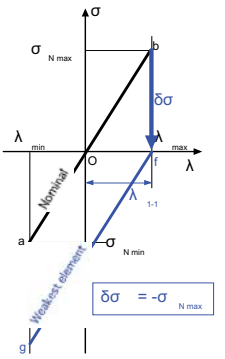

(c) Stress behavour of the weakest bar-element.

Fig. 2 Modelling of plastic adaptation at a surface layer.

viewpoint of macro mechanics. The hypothesis is described as follows. (1) Elastic elongation arising at a maximum stress is transformed into plastic one at a weakest spot in a surface layer, a notch root and a fatigue crack tip. (2) The plastic elongation is restrained with surrounding material and as a result introduces locally an internal compressive stress field. (3) Such an internal compressive stress lowers the actual mean stress value of cyclic stress by being added to the external applied stress. Consequently, elastic energy stored at the maximum stress is relieved in the weakest spot. Therefore, it has been named as the hypothesis of plastic adaptation.

The hypothesis can be reflected in stress-strain hysteresis curves as shown in Fig. 1. A hysteresis curve is transferred at the weakest spot from a site *ab* to a site *gf*, though an outward hysteresis curve remains at a site *ab*. The plastic adaptation is completely finished at the site *gf*. It should be noted that the stress-strain relation *gf* as shown in Fig. 1 is also achieved at the weakest spot in the notch root and the fatigue crack tip in the same way though both stress and strain ranges are expanded by stress concentration. Accordingly, the cyclic stress behaviour at the weakest spot in the notched specimen can be formulated in comparison with that in the unnotched specimen.

The plastic adaptation at a surface layer can be simulated with a parallel multi-bar model as shown in Fig. 2 (a). The bars which are disposed two dimensionally in parallel on a minimum cross-section as shown in Fig. 2 (b) have uniform sectional area and uniform length at the outset. A relation between stress and displacement in the bar *(1,1)* is then shown with a line *ab* in Fig. 2 (c). Now, it is supposed that the bar *(1,1)* disposed at the outside increases plastically in length by elongation corresponding to the maximum displacement of an upper rigid body ($\lambda_{1,1}=\lambda_{max}$). In the model, it is supposed that, without the displacement of the upper rigid body, the increment in length of the bar *(1,1)* is replaced with the elastic body of the same material and of the same dimension as the plastic elongation of the bar *(1,1)*. According to a calculation of a geometric misfit, the cyclic stress behaviour of the bar *(1,1)* is represented by a line *gf* in Fig. 2(c), that is, the mean value of the cyclic stress in the bar *(1,1)* is decreased by $\delta\sigma$ as shown in Eq. (1);

$$\delta\sigma = -\sigma_{N\max} . \qquad (1)$$

On the other hand, the stress range is remained equal to $\Delta\sigma_N$ shown by the line *ab*. In the σ-λ diagram shown in Fig. 2(c), a transfer from the site *ab* to the site *gf* represents the plastic adaptation at the weakest spot of a surface layer.

The hypothesis is applied to problems of proportional multi-axial stress cycling as follows. Three cyclic principal stresses σ_{1N}, σ_{2N} and σ_{3N} which have both maximum and minimum values behave independently on account of the irreversibility of slips for the plastic adaptation and develop the plastic deformation three dimensionally in a pertinent spot. Such deformation leads to local volume expansion, which is restrained by the surrounding material and produces the internal compressive stress field, as a case of cyclic torsion is illustrated in Fig. 3 for an example. Accordingly, the decrease in the mean stress of the weakest spot is estimated by Eq. (2);

$$\delta\sigma^* = -\left(\sigma_{1N\max} + \sigma_{2N\max} + \sigma_{3N\max}\right). \qquad (2)$$

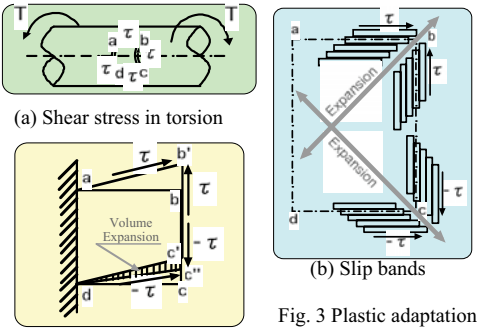

(a) Shear stress in torsion

(b) Slip bands

(c) Volume expansion

Fig. 3 Plastic adaptation by cyclic torsion.

On the other hand, the stress range is calculated as Mises effective stress range by Eq. (3);

$$\Delta\sigma_{eq} = \frac{1}{\sqrt{2}}\sqrt{\left(\Delta\sigma_{1N} - \Delta\sigma_{2N}\right)^2 + \left(\Delta\sigma_{2N} - \Delta\sigma_{3N}\right)^2 + \left(\Delta\sigma_{3N} - \Delta\sigma_{1N}\right)^2}. \qquad (3)$$

Derivation of the R_{EQ}-ratio parameters. R_{EQ}-ratios are derived as parameters for correspondence between cyclic stress conditions of notched and unnotched specimens by developing the unnotched model of Fig. 2 into a notched model as shown in Fig. 4. In Fig. 4 (a), the bars which are disposed in parallel on a notch root cross-section have uniform sectional areas but their initial lengths are in inverse proportion to the stresses distributed on a notch root cross-section, such as $L_1=1/K_t$ for $L_N=1$ where K_t is a theoretical stress concentration factor. Now, provided that the maximum displacement of an upper rigid body λ_{max} is completely replaced in the bar *(1,1)* by plastic deformation $\lambda_{1,1}$, the behaviour of cyclic stress in the bar *(1,1)* is represented with a line *gf* in Fig. 4 (b) from the calculation of the geometric misfit. The displacement $\lambda_{1,1}$ is resolved into two components, i.e., $\lambda'_{1,1}$ for the maximum nominal stress $\sigma_{N\max}$ and $\lambda''_{1,1}$ for the increment of the maximum stress caused by stress concentration $(K_t-1)\sigma_{N\max}$. In Fig. 4(b), these two components are partitioned into by a line *hb* whose maximum stress is equal to $\sigma_{N\max}$. A line *hb* which contains the suppressed plastic deformation $\lambda''_{1,1}$ can be correlated with the stress-displacement relation of the unnotched specimen where, as illustrated in Fig. 4 (c), the initial lengths of all bars are uniformly set equal to $1/K_t$ and are uniformly renewed by adding the length of $\lambda''_{1,1}$ without the displacement of the rigid body and furthermore where the same values of λ_{max} and λ_{min} as those in Fig. 4(b) are alternately repeated. Accordingly, an equation of R_{EQ}-ratio can be derived from the ratio of the minimum stress to the maximum one of the line *hb* in Fig. 4 (b), as follows;

$$R_{EQ} = R_N - (K_t - 1)(1 - R_N), \quad (4)$$

where R_N is a nominal stress ratio and defined by Eq. (5);

$$R_N = \frac{\sigma_{N\min}}{\sigma_{N\max}}. \quad (5)$$

The equations on R_{EQ}-ratios of notched specimens, which are subjected to proportional multiaxial stresses, are derived on the basis on Mises' effective stress and consequently are rewritten by replacing K_t with a Mises' stress concentration factor $K_{t\,eq}$ in Eq. (3). For a circumferential round-bar specimen subjected to torsional loads, $K_{t\,eq} = K_{t\,s}$, where $K_{t\,s}$ is torsional stress concentration factor. For a circumferential notched round-bar specimen subjected to axial loads, $K_{t\,eq} = K_t/p$ where p is a ratio of a sectional average of Mises' effective stress to axial nominal stress. Furthermore, Eq. (5) is rewritten based on Eq. (2) as follows;

$$R^*_N = \frac{\sigma_{1N\min} + \sigma_{2N\min} + \sigma_{3N\min}}{\sigma_{1N\max} + \sigma_{2N\max} + \sigma_{3N\max}}. \quad (6)$$

A value of R^*_N is usually equal to -1 for torsional loads.

The equations of the R_{EQ}-ratios are summarized for individual case of a specimen type and a loading type in Table 1. It must be noted that all equations in Table 1 are applicable to the unnotched specimens by substituting $K_t = K_{t\,s} = K_{t\,eq}$ and $p = 1$.

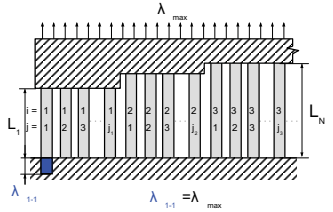

(a) Multi-bar model notch model.

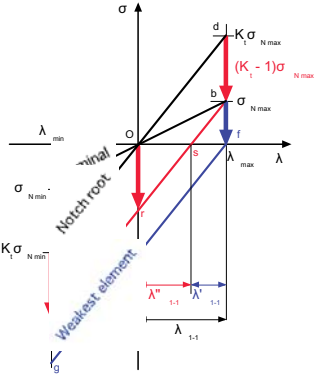

(b) Stress behaviour in the model.

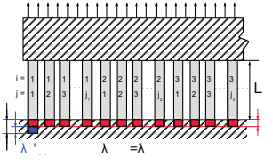

(c) Reproduction model.

Fig. 4 Modelling of plastic adaptation at a notch root.

Table 1 Equations of equivalent stress ratios (R_{EQ}-ratios)

Specimen Type	*Loading Type*	*Equivalent Stress Ratio* R_{EQ}
Notched Plate Specimen	*Axial*	$R_{EQ} = R_N - (K_t - 1)(1 - R_N)$ (R-1)
	Bending	$R_{EQ} = R_N - (K_t - 1)(1 - R_N)$ (R-2)
Notched Round-bar Specimen	*Axial*	$R_{EQ} = R_N - (K_{teq} - 1)(1 - R_N)$ where $K_{teq} \cong K_t/p$ (R-3)
	Bending	$R_{EQ} = R_N - (K_t - 1)(1 - R_N)$ (R-4)
	Torsion	$R_{EQ} = R^*_N - (K_{ts} - 1)(1 - R^*_N)$ where $R^*_N = -1$ (R-5)
	Combined Torsion and Bending	$R_{EQ} = R^*_N - (K_{teq} - 1)(1 - R^*_N)$ (R-6)

$R_N = \frac{\sigma_{N\,min}}{\sigma_{N\,max}}$ *(Nominal Stress Ratio)*

$R^*_N = \frac{\sigma_{1N\,min} + \sigma_{2N\,min} + \sigma_{3N\,min}}{\sigma_{1N\,max} + \sigma_{2N\,max} + \sigma_{3N\,max}}$ *(General Form of Proportional Multiaxial Nominal Stress Ratio)*

$K_t = \frac{\sigma_{NR}}{\sigma_N}$, $K_{ts} = \frac{\tau_{NR}}{\tau_N}$, $K_{teq} = \frac{\sigma_{eqNR}}{\sigma_{eqN}}$ *(Normal, Shear and Mises Effective Stress Concentration Factor)*

$p = \frac{\sigma_{eqN}}{\sigma_N}$ *(Ratio of Sectional Average of Mises Effective Stress to Axial Nominal Stress)*

σ_N, σ_{NR}; *Nominal Stress and Notch-Root-Concentrated Stress*

σ_{1N}, σ_{2N}, σ_{3N}; *Nominal Principal Stresses in Proportional Multiaxial Loading*

σ_{eqN}, σ_{eqNR}; *Nominal Value and Notch-Root-Concentrated Value of Mises Effective Stress*

Method of R_{EQ}-ratio vs. notch-root-concentrated stress range diagramming. The experimental data on the fatigue strength of the notched and unnotched specimens are widely picked up from literature according to the following items;

(1) Influence of notch stress concentration,

(2) Influence of mean stress (notched and unnotched specimens),

(3) Difference of specimen-types (plates and round-bars) and loading type (axial, bending, torsion and their combined loads),

(4) Dependency on materials and their heat- or surface-treated microstructures.

Fatigue data are plotted on the diagrams of R_{EQ}-ratio vs. notch-root-concentrated stress range (R_{EQ}-$\Delta\sigma_{NR}$ diagram) as shown in the flowchart of Fig. 5. Such diagrams represent the character of fatigue strength of the unnotched specimens themselves because the influence of notch stress concentration has been converted as the R_{EQ}-ratio.

The notch-root-concentrated stress range $\Delta\sigma_{NR}$ is calculated from the pertinent equation in Table 2. The $\Delta\sigma_{NR}$ in Table 2 is obtained by multiplying a nominal stress range $\Delta\sigma_N$ by theoretical stress concentration factor. The $\Delta\sigma_{NR}$ for the notched specimen subjected to a torsion and torsion-and-bending combined load is calculated from Kawamoto criterion modified on the basis on Mises criterion. A factor of φ shows a ratio of completely reversed torsion to bending fatigue strength of an unnotched specimen and the value is set at 0.577 in case that it can not be precisely estimated.

Results and Discussion

Fatigue strength diagrams and a notch fatigue criterion. In order to verify the availability of the R_{EQ}-ratio parameter method, the fatigue strength of the notched and unnotched round-bar specimens of SM400 subjected to cyclic axial loading and rotating bending are plotted in Figs. 6 (a), (b) and (c) which show σ_m - $\Delta\sigma_{NR}$, R_N - $\Delta\sigma_{NR}$ and R_{EQ} - $\Delta\sigma_{NR}$ diagrams, respectively. In comparison of Fig. 6 (c) with Figs. 6 (a) and (b), it is found that the parameter of R_{EQ}-ratio is successfully applicable to arrange the fatigue strength data and a certain relation proper to the material is obtained in spite of the difference of notch stress concentration factors and loading types. From Fig. 6(c), a practical criterion on notch fatigue strength can also be obtained as follows. The notch-root-concentrated stress range at the fatigue strength of the notched specimen for any nominal stress ratio R_N is identical with the fatigue strength of the unnotched specimen for the R_{EQ}-ratio;

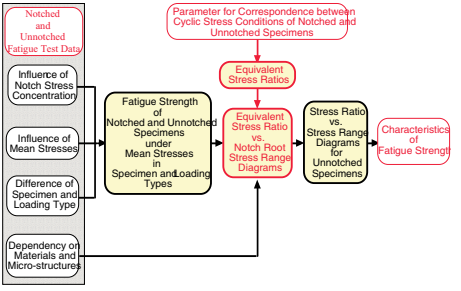

Fig.5 Illustration of R_{EQ}-parameter method.

Table 2 Equations of notch-root-concentration stress ranges.

Specimen Type	*Loading Type*	*Notch-Root-Concentrated Stress Range $\Delta\sigma_{NR}$*	
Notched Plate Specimen	*Axial*	$\Delta\sigma_{NR}=K_t\Delta\sigma_N$	(S-1)
	Bending	$\Delta\sigma_{NR}=K_t\Delta\sigma_{bN}$	(S-2)
Notched Round-bar Specimen	*Axial*	$\Delta\sigma_{NR}=K_t\Delta\sigma_N$	(S-3)
	Bending	$\Delta\sigma_{NR}=K_t\Delta\sigma_{bN}$	(S-4)
	Torsion	$\Delta\sigma_{NR}=K_{ts}\Delta\tau_N$	(S-5)
	Combined Torsion and Bending	$\sqrt{(K_t\Delta\sigma_{bN})^2+(K_{ts}\Delta\tau_N/\varphi)^2}$ $(\varphi\le 1/\sqrt{3})$	(S-6a)
		$\dfrac{(3\varphi^2-1)K_t\Delta\sigma_{bN}+\sqrt{(\varphi^2+1)^2(K_t\Delta\sigma_{bN})^2+16\varphi^2(K_{ts}\Delta\tau_N)^2}}{4\varphi^2}$ $(\varphi\ge 1/\sqrt{3})$	(S-6b)

$\varphi=\tau_w/\sigma_b$ ((Ratio of Completely Reversed Torsion to Bending Fatigue Strength of Unnotched Specimens)

$$K_t\left[\left(\Delta\sigma_N\right)_{w1}\right]_{R_N}=\left[\left(\Delta\sigma\right)_{w0}\right]_{R_{EQ}} \text{ or } \left[\left(\Delta\sigma_{NR}\right)_w\right]_{R_N}=\left[\left(\Delta\sigma\right)_{w0}\right]_{R_{EQ}} \quad (7)$$

In order to confirm the applicability of the R_{EQ}-ratio parameter method to intermediate fatigue life strength, the 10^7 and 2×10^5 cycle fatigue life strength of the notched and unnotched plate specimens of austenitic stainless steel subjected to cyclic axial loading which were conducted by Bell and Benham [1] are plotted on R_{EQ} - $\Delta\sigma_{NR}$ diagrams as shown in Figs. 7(a) and (b), respectively. The diagrams show that the method is applicable to the arrangement of intermediate fatigue life strength.

Fatigue strength data of the notched and unnotched round-bar specimens of low carbon steel subject to axial, bending, torsion and their proportional combination loading, which were conducted by Kawamoto [2] and Kawamoto and Seki [3], are plotted on the R_{EQ} - $\Delta\sigma_{NR}$ diagrams as shown in Fig. 8, and the influence of different loading types are examined. It is found that a certain relation proper to the tested material is obtained in spite of the difference of the loading type.

Discrimination of fatigue strength σ_{w1} and σ_{w2}. Frost and Dugdale [4] carried out axial loading fatigue tests on mild steel plate specimens containing edge notches of various root radii. Tests were performed both with zero mean load and with various superimposed tensile and compressive mean loads. They examined metallurgically the sections of notch roots of unbroken specimens after fatigue tests and classified fatigue test results into three groups: (1) Broken, (2) Unbroken but cracked (non-propagation cracked) and (3) Uncracked. From this classification, they described presence of two types of fatigue strength: (1) Stress required to initiate a crack (it is generally named as fatigue strength σ_{w1}) and (2) Stress required to propagate a crack (it is generally named as fatigue strength σ_{w2}). It is however very difficult to discriminate between initiation and propagation of a fatigue crack. We can often observe in the fatigue test of the unnotched specimen that microscopic fatigue cracks are left at the surface under cyclic stresses slightly less than σ_{w1}. As described later, the σ_{w1} and σ_{w2}

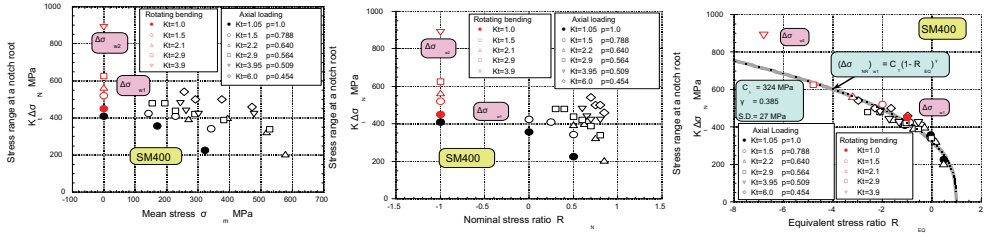

(a) σ_m-based diagram. (b) R_N-based diagram. (b) R_{EQ}-based diagram.

Fig. 6 Availability of R_{EQ}−parameter method for diagramming fatigue strength (SM400).

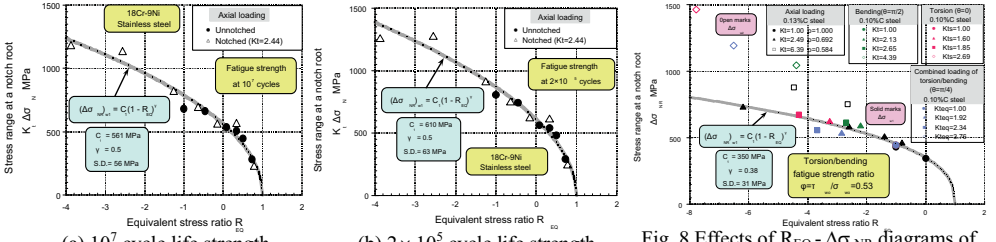

(a) 10^7 cycle life strength. (b) 2×10^5 cycle life strength.

Fig. 8 Effects of R_{EQ} - $\Delta\sigma_{NR}$ diagrams of low carbon steel on loading types [2,3].

Fig. 7 R_{EQ} - $\Delta\sigma_{NR}$ diagrams of austenite stainless steel [1].

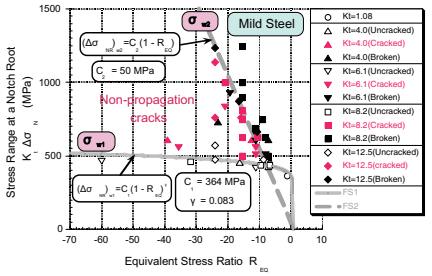

Fig. 9 Fatigue strength σ_{w1} and σ_{w2} on R_{EQ} - $\Delta\sigma_{NR}$ diagrams of mild steel [4].

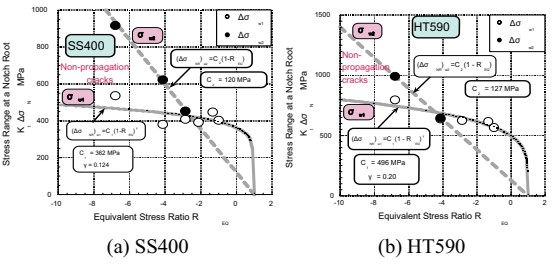

(a) SS400 (b) HT590

Fig. 10 Fatigue strength σ_{w1} and σ_{w2} on R_{EQ} - $\Delta\sigma_{NR}$ diagrams of SS400 and HT590 [5].

reflect the difference between the mechanisms of fatigue crack growth rather than that between the fatigue processes of crack initiation and growth.

Fig. 9 shows R_{EQ} - $\Delta\sigma_{NR}$ diagram on the fatigue tests conducted by Frost and Dugdale [4]. In the diagram, a curved line between open and red-colored solid marks represents σ_{w1} and a straight line between red- and black-colored solid marks does σ_{w2}. The fatigue strength is transferred from σ_{w1}- to σ_{w2}-type at a low R_{EQ}-ratio condition. Watanabe et al. [5] conducted out-of-plane bending fatigue tests of notched and unnotched plate specimens of mild steel (SS400) and high tensile steel (HT590) in order to examine material-dependency of σ_{w1} and σ_{w2}. Figs. 10 (a) and (b) show the R_{EQ} - $\Delta\sigma_{NR}$ diagrams of SS400 and HT590, respectively. In comparison, high tensile steel is improved more in σ_{w1} rather than in σ_{w2}. As a result, R_{EQ}-ratio transferring from σ_{w1}- to σ_{w2}-type is lower in HT590 than in SS400 and the region on non-propagation crack become narrower in HT590 than in SS400.

Fatigue strength diagrams of heat- and surface-treated steels. Carbon steels and their alloy steels are often subjected to heat- and surface-treatment for the purpose of strengthening. In order to examine influences of heat- and surface-treatment on fatigue strength σ_{w1} and σ_{w2}, fatigue data of S45C are picked up from JSMS database [6] and plotted on R_{EQ} - $\Delta\sigma_{NR}$ diagram as shown in Fig. 11. In the region plotted, σ_{w1} is only exhibited under annealed and normalized conditions, and both σ_{w1} and σ_{w2} are exhibited under quenched-tempered conditions though they tend to be lower as tempering temperatures are higher. Both σ_{w1} and σ_{w2} are remarkably heightened under induction-hardened conditions without post heat-treatment. It should be noted that R_{EQ}-ratio transferring from σ_{w1} to σ_{w2}-type is very high under induction-hardening conditions and the transition is furthermore followed by decrease in fatigue strength. Such decrease in fatigue strength due to the transition from σ_{w1} to σ_{w2}-type is exhibited more remarkably in high strength steel SNCM439 tempered at low temperatures after quenched, as shown in Fig. 12.

Itoga et al. [7] conducted cantilever rotary bending tests of notched and unnotched specimens of high strength steel SNCM439 which was tempered at 200 °C × 1hr and subsequently air-cooled after quench, and the experimental data are plotted on R_{EQ} - $\Delta\sigma_{NR}$ diagram in Fig. 12 by using black- and red- colored solid marks. The fatigue data picked up from JSMS database are plotted by open marks. The open round marks show fatigue strength of unnotched specimens tempered at 280 °C × 1hr and subsequently

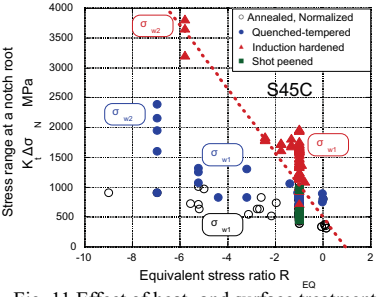

Fig. 11 Effect of heat- and surface treatment R_{EQ} - $\Delta\sigma_{NR}$ diagrams of S45C steels [6].

oil-cooled after quench. Attending to the black-colored solid marks, which represent the fatigue strength for surface fracture of specimens, the transition from σ_{w1} to σ_{w2}-type brings about sharp decrease in fatigue strength. This means that σ_{w1} and σ_{w2} do not reflect difference between fatigue processes of crack initiation and growth but do difference between mechanisms of fatigue crack growth in an early stage. The transition is explained as follows; (1) Quenching introduces a large abundance of dislocations and increases slip resistance due to back stress of piled-up dislocations. As a result fatigue strength is increased. (2) Once dislocations begin to move, multiple slips are induced and density of dislocations is lowered rapidly by annihilation. Such a process is exhibited as cyclic strain softening. (3) Annihilation of dislocations produces a large amount of vacancies and interstitial type interface dislocations and contributes to expansion of slip band. The expansion is restrained and induces internal compressive stress into the slip band. As a result, fatigue strength exhibits strong mean stress dependency. (4) It is generally thought that the back stress effect of dislocations is larger at comparatively lower stress range levels and the annihilation effect is larger at comparatively higher stress range levels. It is however guessed that very high stress ranges introduced into heat- and surface-treated materials unstabilize and/or collapse the balance between back stress and annihilation effects of dislocations and consequently bring an irregular transition from σ_{w1} to σ_{w2}.

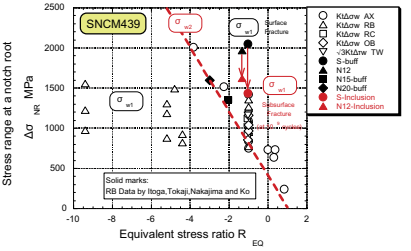

Fig. 12 R_{EQ} - $\Delta\sigma_{NR}$ diagrams of heat- and surface-treated SNCM439 steels [6,7]

The red-colored solid marks in Fig. 12 represent the fatigue life strength defined at 10^9 cycles for subsurface fracture. Subsurface fracture was brought about in unnotched and the bluntest notched specimens. The fatigue strength is remarkably lowered from σ_{w1} and it seems to approach σ_{w2} with increase in cycles. It seems that it is reasonable to regard the fatigue strength for subsurface fracture as σ_{w2}.

Summary

A new method for diagramming fatigue strength on the basis of the equivalent stress ratios (R_{EQ}-ratios) is proposed and applied to various kinds of steels. Fatigue strength diagrams are characterized with two characters of fatigue strength σ_{w1} and σ_{w2}. The proposed method is successfully to estimation of fatigue strength of heat- and surface-treated material.

References

[1] W.J. Bell and P.P. Benham: ASTM STP 338 (1962), p. 25.
[2] M. Kawamoto: J. Japan Soc. Testing Materials, Vol. 2 (1953), p. 85.
[3] M. Kawamoto and M. Seki: J. Japan Soc. Testing Materials, Vol. 4 (1955), p. 571.
[4] N.E. Frost and D.S. Dugdale: J. Mech. Phys. Solids, Vol. 5 (1957), p. 182.
[5] M. Watanabe, K. Nagai, T. Yamaguchi and S. Hioki: J. Japan Weld. Soc. Vol. 36 (1967), p. 32.
[6] Edit. Japan Soc. Mat. Sci.: Databook on Fatigue Strength of Metallic Materials (1996), Elsevier.
[7] H. Itoga, K. Tokaji, M. Nakajima and H.N. Ko: J. Soc. Mat. Sci. Japan, Vol. 54 (2005), p. 1249.